

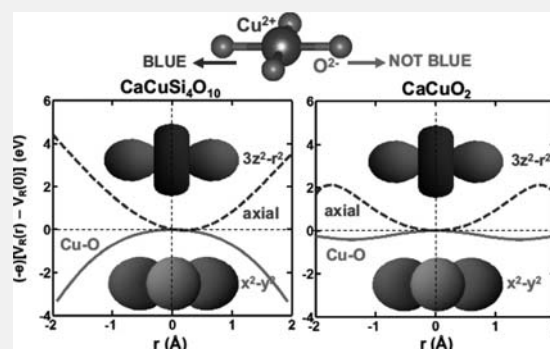
Origin of the Exotic Blue Color of Copper-Containing Historical Pigments

Pablo García-Fernández,* Miguel Moreno, and José Antonio Aramburu

Departamento de Ciencias de la Tierra y Física de la Materia Condensada, Universidad de Cantabria, Avenida de los Castros s/n, 39005 Santander, Spain

Supporting Information

ABSTRACT: The study of chemical factors that influence pigment coloring is a field of fundamental interest that is still dominated by many uncertainties. In this Article, we investigate, by means of ab initio calculations, the origin of the unusual bright blue color displayed by historical Egyptian Blue ($\text{CaCuSi}_4\text{O}_{10}$) and Han Blue ($\text{BaCuSi}_4\text{O}_{10}$) pigments that is surprisingly not found in other compounds like $\text{BaCuSi}_2\text{O}_6$ or CaCuO_2 containing the same CuO_4^{6-} chromophore. We show that the differences in hue between these systems are controlled by a large red-shift (up to 7100 cm^{-1}) produced by an electrostatic field created by a lattice over the CuO_4^{6-} chromophore from the energy of the $3z^2-r^2 \rightarrow x^2-y^2$ transition, a nonlocal phenomenon widely ignored in the realm of transition metal chemistry and strongly dependent upon the crystal structure. Along this line, we demonstrate that, although SiO_4^{4-} units are not involved in the chromophore itself, the introduction of sand to create $\text{CaCuSi}_4\text{O}_{10}$ plays a key role in obtaining the characteristic hue of the Egyptian Blue pigment. The results presented here demonstrate the opportunity for tuning the properties of a given chromophore by modifying the structure of the insulating lattice where it is located.



INTRODUCTION

Dyes and pigments have a variety of applications and are in huge demand in industry.¹ However, obtaining stable pigments that display particular tonalities has often proven difficult as many nonquantified factors are involved in the chemistry of color.^{1–7} Thus, understanding how to modify the hue of a chromophore while retaining strong chemical stability is crucial, as this knowledge would allow a bottom-up approach to pigment design. In this Article, we study the origin of historical pigment colors used in ancient Egyptian and Chinese civilizations based on square-planar CuO_4^{6-} complexes, with extra attention paid to those displaying an unusual bright blue tonality.^{2–4} Our primary finding is that, in all of these systems, the color is unexpectedly controlled by an electrostatic field that is created by the lattice over the CuO_4^{6-} chromophore. This key factor, however, is usually ignored in the large body of work in the field of transition metal chemistry, where properties are usually explained considering only the complex at equilibrium geometry.^{5–11}

Historically, the technology of pigments was amongst the earliest that mankind developed.^{2–4} By using different colored earth, or grinding soft rocks to a powder, prehistoric humans could make pictures of different colors, such as the wonderful drawings in Altamira (Spain) and Lascaux (France) caves. Interestingly, the color blue is absent in prehistoric paintings because of its scarcity in surface soils. Blue pigments only began to appear in human history when mining was developed, and

even then they remained rare. This was the case for lapis lazuli, a blue-colored stone that was found only in one mine for the whole ancient world, which is located in modern-day Afghanistan.^{2–4}

The first traces of man-made blue pigments date back to early Egyptian culture (predynastic era, $\sim 3600\text{ BC}$) where the so-called Egyptian Blue pigment was prepared. This first synthetically produced pigment in human history involves a mixture containing several phases, including cuprorivaite ($\text{CaCuSi}_4\text{O}_{10}$), unreacted quartz, and variable amounts of glass.^{2–4,12} The exotic bright blue color of the pigment is due to the square-planar CuO_4^{6-} chromophore^{2–4,8,12} present in the insulating $\text{CaCuSi}_4\text{O}_{10}$ compound displaying the gillespite ($\text{BaFeSi}_4\text{O}_{10}$) structure¹³ (tetragonal space group $P4/ncc$, see Figure 1). The Egyptian Blue pigment is very stable, was used extensively for decorative purposes in the early dynasties in Egypt (until the end of the Roman period), Greece, and around the Roman Empire, and can be found, for example, in Amarna, Luxor, the Parthenon, and Pompeii.¹⁴ As a remarkable example, pure Egyptian Blue was used in the crown of a famous bust of Queen Nefertiti.^{2–4}

Significantly later, and most likely developed independently,¹⁵ two pigments involving a colored compound with a composition somewhat similar to that of cuprorivaite were

Received: August 29, 2014

Published: December 17, 2014

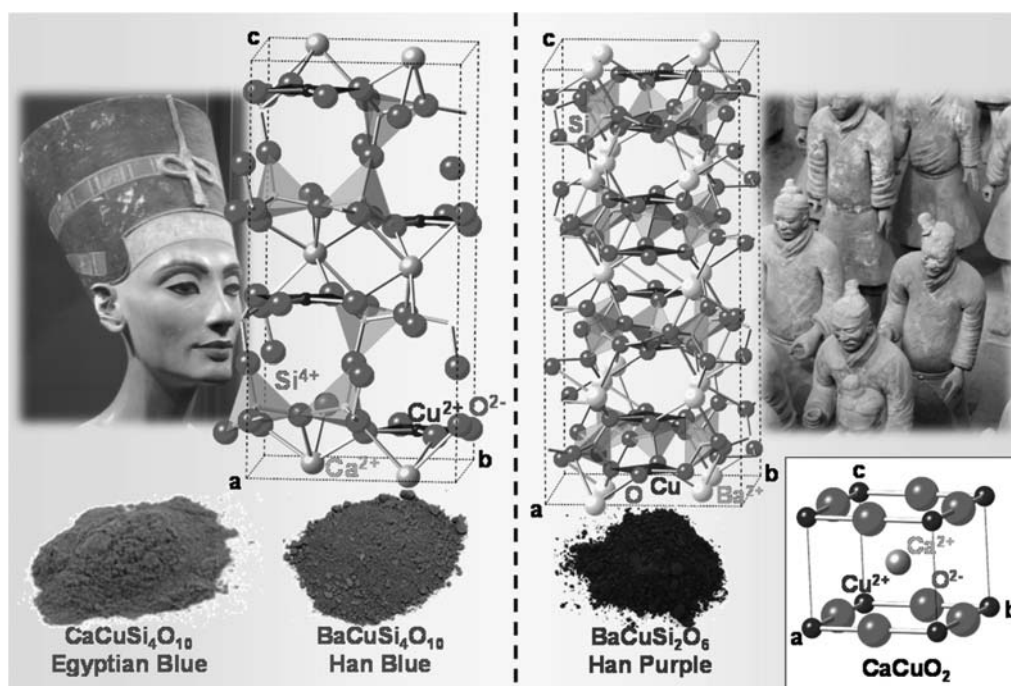


Figure 1. Unit cells corresponding to Egyptian Blue ($\text{CaCuSi}_4\text{O}_{10}$) and Han Blue ($\text{BaCuSi}_4\text{O}_{10}$) pigments (left), the Han Purple ($\text{BaCuSi}_2\text{O}_6$) pigment (right), and the CaCuO_2 compound (white box). Cu^{2+} ions involved in square-planar CuO_4^{6-} complexes are depicted in dark blue, whereas SiO_4^{4-} tetrahedrons are in green.

Table 1. Experimental Values of the $\text{Cu}^{2+}-\text{O}^{2-}$ Distances, R (Å), and Peak Energies (cm^{-1}) of the Three d-d Transitions for Compounds Containing Square-Planar CuO_4^{6-} Complexes

	$\text{CaCuSi}_4\text{O}_{10}$ (Egyptian Blue)	$\text{BaCuSi}_4\text{O}_{10}$ (Han Blue)	$\text{BaCuSi}_2\text{O}_6$ (Han Purple)	CaCuO_2	Li_2CuO_2
space group	$P4/ncc$	$P4/ncc$	$P4_1/acd$	$P4/mmm$	$Immm^a$
R	1.928 ^b	1.921 ^b	1.945 ^c	1.929 ^d	1.959 ^e
$b_{2g}(xy) \rightarrow b_{1g}(x^2-y^2)$	12740 ^f	12900 ^g	13500 ^h	13220 ⁱ	14000 ^j
$e_g(xz,yz) \rightarrow b_{1g}(x^2-y^2)$	16130 ^f	15800 ^g	17000 ^h	15720 ⁱ	17000 ^j
$a_{1g}(3z^2-r^2) \rightarrow b_{1g}(x^2-y^2)$	18520 ^f	18800 ^g	$\sim 21000^h$	21370 ⁱ	$\sim 21900^j$

^aSee structure in the Supporting Information. ^bFrom ref 13. ^cFrom ref 16. ^dFrom ref 22. ^eFrom ref 23. ^fFrom refs 9, 18–20, and 24. ^gFrom ref 8. ^hFrom ref 25. ⁱFrom ref 11. ^jFrom ref 10.

employed during the Han dynasty (208 BC–220 AD) in China.^{3,4} The color of the so-called Han Blue pigment is also bright blue due to $\text{BaCuSi}_4\text{O}_{10}$, which has the same gillespite structure as cuprorivaite¹³ (Figure 1). In contrast, a different color is exhibited by the Han Purple pigment, which was identified in Terracotta Warriors discovered in central China in 1974 and is based on $\text{BaCuSi}_2\text{O}_6$. This compound belongs to the $P4_1/acd$ space group¹⁶ (Figure 1) that also involves square-planar CuO_4^{6-} chromophores. A similar situation holds for Li_2CuO_2 and CaCuO_2 compounds, which have d-d transition energies that are certainly different^{10,11} than those measured for $\text{CaCuSi}_4\text{O}_{10}$ and $\text{BaCuSi}_4\text{O}_{10}$, though they also contain square-planar CuO_4^{6-} complexes.

Despite the indisputable importance of the Egyptian Blue pigment in history, art, and archeological studies, as well as in current applications,¹⁷ the actual origin of the unusual blue color displayed by $\text{CaCuSi}_4\text{O}_{10}$ and $\text{BaCuSi}_4\text{O}_{10}$ pigments is not yet understood. This Article aims to explain, by means of ab initio calculations, why d-d transitions of $\text{CaCuSi}_4\text{O}_{10}$, CaCuO_2 , and $\text{BaCuSi}_2\text{O}_6$ are so different despite the compounds having the same CuO_4^{6-} chromophore.

Compounds containing square-planar CuO_4^{6-} complexes have three broad d-d bands (bandwidth $\sim 2500 \text{ cm}^{-1}$) in the optical region that cover most of the spectrum. Table 1 shows experimental structural and optical data in these systems.^{9,10,13,16,18–25} In particular, it contains the peak energies of the three d-d bands corresponding to Egyptian Blue, Han Blue, and Han Purple pigments as well as those measured for CaCuO_2 and Li_2CuO_2 compounds, which display a simpler crystal structure^{22,23} and have interesting electrical and magnetic properties.^{26–28}

As shown in Table 1, when comparing Egyptian and Han Blue pigments with the rest of the compounds containing square-planar CuO_4^{6-} complexes, we found that the peak energy of the band corresponding to the highest $a_{1g}(3z^2-r^2) \rightarrow b_{1g}(x^2-y^2)$ excitation, denoted $E(z^2)$, is lowered by approximately 3000 cm^{-1} , thus opening up a gap in the blue region ($\sim 21500 \text{ cm}^{-1}$) not present in the other systems. Because the rest of the visible spectrum is absorbed by the three broad d-d transitions, this gives rise to the characteristic bright blue color exhibited by such pigments (Figure 1).

Almost without exception, the spectra of transition metal complexes in insulating compounds are analyzed based solely

on the chemical nature of the ligands and their distance to the central metal cation.^{5–11} However, as shown below, this widely used approach is unable to explain the different energies observed for d-d transitions of the historical blue pigments when compared with those of compounds like CaCuO₂ or CaCuSi₂O₆, all of which involve square-planar CuO₄⁶⁻ complexes. For example, the effect of chemical substitution of ligands in octahedral complexes is usually accounted for using the spectrochemical series.²⁹ In this case, taking the experimental value³⁰ of $E(z^2) = 16990 \text{ cm}^{-1}$ for the square-planar CuCl₄²⁻ chromophore in (N-mph)₂CuCl₄, it could be expected²⁹ simply that when chlorine is replaced by oxygen as the ligand, $E(z^2)$ should be around 22000 cm⁻¹. This figure, however, is far from the experimental value for Egyptian Blue and Han Blue pigments but rather is close to that measured for CaCuO₂¹¹ and Li₂CuO₂¹⁰ as shown in Table 1. The 14% reduction in $E(z^2)$ when comparing CaCuO₂ and CaCuSi₄O₁₀ could be explained within the ligand field theory²⁹ only if the Cu²⁺–O²⁻ distance, R , is smaller for the former than for the latter compound due to the strong R dependence of the splitting among d -levels. However, X-ray diffraction measurements^{13,22} show that the R value of 1.928 Å for the Cu²⁺–O²⁻ distance in CaCuSi₄O₁₀ is coincident within 0.05% with the R value of 1.929 Å corresponding to CaCuO₂ (Table 1). Furthermore, as the Cu²⁺–O²⁻ distance in Egyptian Blue is smaller than that measured for Li₂CuO₂ ($R = 1.959 \text{ Å}$)²³ or BaCuSi₂O₆ ($R = 1.945 \text{ Å}$),¹⁶ it could be expected from ligand field theory that $E(z^2)$ should be higher for the former than for the latter compound. As these conclusions are all contradictory to experimental data, this clearly proves the failure of the ligand field theory for the present insulating compounds. Therefore, the optical properties of blue pigments cannot be explained through only the CuO₄⁶⁻ complex at the correct R value, even though active electrons are actually localized in it.

The primary goal of this Article is to clarify this puzzling issue on the basis of recent results on fluorides containing CuF₆⁴⁻ units.³¹ Indeed, in systems like K₂CuF₄ and K₂ZnF₄:Cu²⁺, it has been proven that the energy of d-d transitions is also influenced by the electrostatic potential $V_R(\mathbf{r})$ created by the other lattice ions upon the active electrons actually confined in the CuF₆⁴⁻ complex. Accordingly, we explore here whether the differences observed for the d-d transitions in CuO₄⁶⁻ complexes embedded in CaCuSi₄O₁₀, CaCuO₂, and BaCuSi₂O₆ can be accounted for by the same mechanism.

COMPUTATIONAL DETAILS

Geometry optimizations of the compounds have been carried out by means of periodic ab initio calculations based on density functional theory (DFT) using the CRYSTAL09 package that employs localized Gaussian-type orbital (GTO) basis sets to represent the Bloch orbitals.³² With regard to the basis sets, most of the calculations were performed using the pob-TZVP-2012 functions recently optimized by Peintinger, Oliveira, and Bredow,³³ which are all-electron with triple- ζ valence with polarization quality. With regard to the exchange–correlation functionals, we have employed the hybrid functionals B1WC,³⁴ PW1PW,³⁵ and B3LYP³⁶ (with 16, 20, and 30% Hartree–Fock exchange, respectively). These hybrid functionals allow us to obtain geometries, band gaps, and thermochemical properties with great accuracy and reliability without the need for semiempirical parameters like in DFT+U procedures. Results using the three functionals are similar, with smaller than 1 pm differences in the Cu²⁺–O²⁻ bond distances, which is not surprising because this bond is rather strong. We have employed an $8 \times 8 \times 8$ k-point mesh, and the

structures have been relaxed until a maximum force value below 0.02 eV/Å and a total energy change below 10⁻⁷ eV were obtained.

As an example of the reliability of the present periodic calculations, carrying them out on CaCuSi₄O₁₀ is found to reproduce the experimental lattice parameters ($a = 7.3017 \text{ Å}$, $c = 15.1303 \text{ Å}$) and the Cu²⁺–O²⁻ distance ($R = 1.929 \text{ Å}$) with errors of <0.7%. Similar deviations are found in the calculations on CaCuO₂, where experimental values are $a = 3.856 \text{ Å}$, $c = 3.180 \text{ Å}$, and $R = 1.928 \text{ Å}$. Calculated lattice parameters of the other compounds are reported in the Supporting Information.

Energies of the d-d electronic transitions of the copper systems have been calculated through the cluster approach by means of version 2013.01 of the Amsterdam density functional (ADF) code³⁷ using the energy difference from two fully converged total-energy calculations with the appropriate electronic configuration. As active electrons are confined in the CuO₄⁶⁻ unit (our periodic calculations yield <2% of the active electrons outside these ions), calculations have been performed on a simple CuO₄⁶⁻ complex but subject to the electrostatic potential $V_R(\mathbf{r})$ that is created by the rest of the lattice ions. For these calculations, we have used the popular B3LYP hybrid functional³⁶ in the spin-unrestricted Kohn–Sham formalism of the DFT and high-quality all-electron basis sets of triple- ζ plus polarization (TZP). We have verified that similar results are obtained using other hybrid functionals, including B1WC, PW1PW, and mPW1PW (with 16, 20, and 42.8% Hartree–Fock exchange, respectively). Calculation of electrostatic potentials $V_R(\mathbf{r})$ in the complex region was performed with the well-known Ewald method^{38,39} using a modified formula to facilitate computational calculations. More details on the particular implementation can be found in ref 38. In a second step, the potential in that region has been reproduced using ~200 fictitious charges lying outside the region. Finally, these fictitious charges were placed into the ADF calculations to produce the lattice embedding for the CuO₄⁶⁻ complexes.

The values of the ionic charges in this calculation were obtained from ab initio simulations. We have checked that the resulting potential is essentially nondependent on the criterion (e.g., nominal, Mulliken, Bader) used to obtain the charges.³¹

RESULTS AND DISCUSSION

For the sake of clarity, we have first explored whether or not the different d-d spectra of CaCuSi₄O₁₀ and CaCuO₂ can be explained by the different electrostatic potentials $V_R(\mathbf{r})$ felt by electrons confined in the CuO₄⁶⁻ complex. For this reason, we have calculated the d-d transitions corresponding to a single CuO₄⁶⁻ complex at $R = 1.928 \text{ Å}$ under the influence of distinct $V_R(\mathbf{r})$ potentials corresponding to CaCuSi₄O₁₀ and CaCuO₂. As shown in Table 2, the different d-d transitions observed in

Table 2. Calculated Energies (cm⁻¹) of the d-d Transitions for Egyptian Blue (CaCuSi₄O₁₀) and CaCuO₂

transitions	CuO ₄ ⁶⁻ + $V_R(\mathbf{r})^a$		extrapolation to zero-field CuO ₄ ⁶⁻ ^b
	CaCuSi ₄ O ₁₀ ^c	CaCuO ₂ ^d	
kb _{2g} (xy) → b _{1g} (x ² -y ²)	12010	12400	~14100
	(12740)	(13230)	
e _g (xz,yz) → b _{1g} (x ² -y ²)	15970	15600	~18800
	(16130)	(15730)	
a _{1g} (3z ² -r ²) → b _{1g} (x ² -y ²)	19600	22180	~26700
	(18500)	(21375)	

^aAdding the electrostatic potential $V_R(\mathbf{r})$ ($\lambda = 1$) of the CaCuSi₄O₁₀ and CaCuO₂ lattices. ^bExtrapolation to the zero-field limit for the CuO₄⁶⁻ complex at $R = 1.928 \text{ Å}$ using the data in Figure 2. ^cExperimental values from refs 9, 18–20, and 24 are given in parentheses. ^dExperimental values from ref 11 are given in parentheses.

$\text{CaCuSi}_4\text{O}_{10}$ and CaCuO_2 are very reasonably reproduced by the present calculations, thus stressing the key role played by the internal $V_R(\mathbf{r})$ potential. This contrasts with explanations^{5–11} based on metal–ligand distance or hybridization changes inside the complex that are usually employed in the literature on transition metal systems.

Seeking to further explore the influence of the internal potential on the d-d transitions, we studied their sensitivity to the field using the rescaled potential $\lambda V_R(\mathbf{r})$. As shown in Figure 2, the variation around $\lambda = 1$ is linear for both $\text{CaCuSi}_4\text{O}_{10}$ and

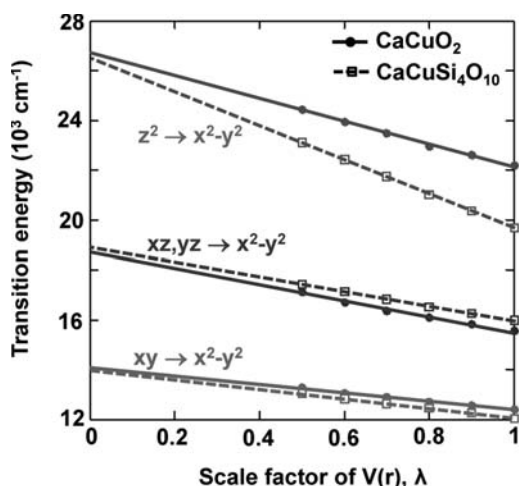


Figure 2. Variation of the three d-d transition energies for a square-planar CuO_4^{6-} complex subjected to scaled embedding potential $\lambda V_R(\mathbf{r})$. Filled circle and empty square markers correspond to calculated energies using a TZP basis set in the $0.5 \leq \lambda \leq 1$ range for CaCuO_2 and $\text{CaCuSi}_4\text{O}_{10}$, respectively. The linear tendency plots (very similar for TZP, TZ2P, and QZP basis sets) extrapolated for the complete $0 \leq \lambda \leq 1$ range obtained for CaCuO_2 and $\text{CaCuSi}_4\text{O}_{10}$ are shown by means of solid and dashed lines, respectively.

CaCuO_2 . We have checked that the slope of this line is very similar for various basis sets. For moderately large TZP basis sets, this tendency extends over the $0.5 \leq \lambda \leq 1$ range for both lattices; however, when $\lambda \leq 0.4$, the calculations stop converging. This result is consistent with the fact that the isolated CuO_4^{6-} complex is unstable. Indeed, this species is highly negatively charged and thus requires being embedded in a lattice to become stable. Despite this fact, if we extrapolate the results obtained for a given d-d transition of the CuO_4^{6-} complex to the zero-field limit ($\lambda = 0$, Figure 2), we find the same value for the $\text{CaCuSi}_4\text{O}_{10}$ and CaCuO_2 compounds.

Therefore, the results obtained in the zero-field limit taken in this way can be considered as a reference that could be interpreted as transitions for an in vacuo complex. Thus, this mathematical extrapolation provides some foundation to the idea of complex in vacuo often employed when discussing the optical or magnetic properties of insulating transition metal compounds⁴⁰ even when the species is not stable.

As shown in Figure 2 and Table 2, the d-d transition with the highest energy is always $a_{1g}(3z^2-r^2) \rightarrow b_{1g}(x^2-y^2)$, a situation quite different from that encountered in a distorted octahedral unit³¹ due to the lack of axial ligands in a true square-planar complex. Optical data on the square-planar CuCl_4^{2-} unit in $(\text{N-nph})_2\text{CuCl}_4$ reveal that the $a_{1g}(3z^2-r^2) \rightarrow b_{1g}(x^2-y^2)$ transition has the highest energy among the ensemble of d-d transitions.³⁰

We observe in Table 2 that although the calculations predict that $E(z^2)$ would be equal to $\sim 26700 \text{ cm}^{-1}$ for the CuO_4^{6-} complex at $R = 1.928 \text{ \AA}$ in the referenced zero-field limit, the addition of the lattice potential $V_R(\mathbf{r})$ induces a dramatic reduction in the $E(z^2)$ energy equal to 4520 cm^{-1} for CaCuO_2 and to 7100 cm^{-1} for $\text{CaCuSi}_4\text{O}_{10}$. The results in Table 2 thus clearly show that the calculated transition energies are strongly sensitive to the $V_R(\mathbf{r})$ potential, the inclusion of which is completely necessary for accurate prediction of their energies. This improvement is particularly dramatic for $a_{1g}(3z^2-r^2) \rightarrow b_{1g}(x^2-y^2)$. This conclusion thus concurs with recent findings for CuF_6^{4-} complexes in insulating fluorides like K_2CuF_4 and $\text{K}_2\text{ZnF}_4:\text{Cu}^{2+}$, where the electrostatic potential $V_R(\mathbf{r})$ has been proven to play a key role in explaining the experimental d-d transitions.³¹ In the same vein, the different colors displayed by ruby and emerald, two gemstones with the same CrO_6^{9-} chromophore, are due to the different $V_R(\mathbf{r})$ shapes in Al_2O_3 and $\text{Be}_3\text{Si}_6\text{Al}_2\text{O}_{18}$ host lattices⁴¹ and not to different $\text{Cr}^{3+}-\text{O}^{2-}$ distances^{41,42} as has widely been assumed.^{5,6} Additional results on the influence of $V_R(\mathbf{r})$ on other compounds containing CuO_4^{6-} complexes are provided in the Supporting Information.

Because the effects of $V_R(\mathbf{r})$ upon the d-d transitions depend on the anisotropy of $V_R(\mathbf{r})$ in the complex region, we need to study the behavior of the quantity $(-e)[V_R(\mathbf{r}) - V_R(0)]$, where $V_R(0)$ is the potential at the copper site. To qualitatively understand the strong and differentiated effect of $(-e)[V_R(\mathbf{r}) - V_R(0)]$ over the $a_{1g}(3z^2-r^2) \rightarrow b_{1g}(x^2-y^2)$ transition in $\text{CaCuSi}_4\text{O}_{10}$ and CaCuO_2 crystals, it is worth noting that the orbitals involved in the electron excitation are directed in orthogonal directions. The lower $a_{1g}(3z^2-r^2)$ orbital is mainly localized in an axis perpendicular to the CuO_4^{6-} complex plane, whereas the $b_{1g}(x^2-y^2)$ orbital is contained within this plane and has its maximum density along the Cu–O bond direction. Plotting the potential along these directions (Figure 3), we find that both the in-plane and out-of-plane components of the field are qualitatively similar in $\text{CaCuSi}_4\text{O}_{10}$ and CaCuO_2 , favoring the reduction of energy for the higher x^2-y^2 orbital and increasing it for the perpendicular $3z^2-r^2$ orbital, and thus decrease the $a_{1g}(3z^2-r^2) \rightarrow b_{1g}(x^2-y^2)$ transition energy. However, the intensity of $(-e)[V_R(\mathbf{r}) - V_R(0)]$ is different in each case, being much stronger in Egyptian Blue than in CaCuO_2 , leading to a more substantial reduction of $E(z^2)$ and to the opening of a gap that prevents the absorption of blue light by $\text{CaCuSi}_4\text{O}_{10}$. Thus, these results clearly show how crystal structures (Figure 1) can create distinct and strongly anisotropic $V_R(\mathbf{r})$ potentials around a chromophore, modulating its energy levels in different ways to control the color the system displays.

We would like to stress here that many authors⁴³ have indicated that the different optical spectra in this kind of system are mainly due to differences in the local $3d(3z^2-r^2)-4s$ hybridization of the transition metal, lowering the position of the $a_{1g}(3z^2-r^2)$ level with respect to that of $b_{1g}(x^2-y^2)$. This conclusion has been reached through the use of parametrized semiempirical models (e.g., the angular overlap model), introducing ad hoc parameters for the effects under consideration and fitting them to reproduce the experimental data.⁴⁴ On the other hand, our calculations show that toward the zero-field limit the $3d(3z^2-r^2)-4s$ hybridization in $\text{CaCuSi}_4\text{O}_{10}$ and CaCuO_2 is exactly the same, and as a consequence, the chemical factor inducing the appearance of small differences in hybridization is the presence of the field. In particular, we have obtained similar values of 5 and 7% mixtures

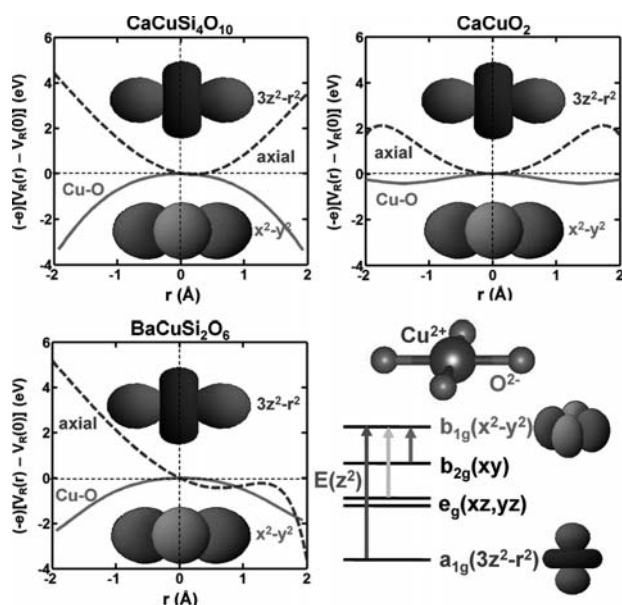


Figure 3. Variation of $(-e)[V_R(r) - V_R(0)]$ potential energy felt by an electron of the CuO_4^{6-} complex when the electron coordinate r moves along either the in-plane Cu–O bond (solid red lines) or the axial OZ (dashed blue lines) direction, primarily perturbing the $b_{1g}(x^2-y^2)$ and $a_{1g}(3z^2-r^2)$ orbitals, respectively. Results for $\text{CaCuSi}_4\text{O}_{10}$, $\text{BaCuSi}_2\text{O}_6$, and CaCuO_2 crystals are reported. In all cases, data for the axial domain with $r > 0$ correspond to the region of the compound just above the complex in the unit cell of Figure 1 with the lowest value of the Z coordinate. A scheme of the d-d transitions for the CuO_4^{6-} complex is also shown at the bottom right.

of $4s(\text{Cu})$ character for $\text{CaCuSi}_4\text{O}_{10}$ and CaCuO_2 , respectively, into the $a_{1g}(3z^2-r^2)$ orbital, reflecting the higher confinement of the $3z^2-r^2$ orbital due to the field in the first system with respect to the second. Moreover, from an energetic point of view, we see that changes of the transitions are linear with the field (Figure 2), a clear indication that the effects of these hybridizations, which would show as a quadratic contribution to the level's energies, are small. In summary, our results show that although there is some correlation between changes in the spectrum and 3d-4s hybridization, the latter cannot be considered the cause of the former because (a) both effects appear with the introduction of the field and (b) the optical changes follow the effect of the embedding potential linearly instead of quadratically, which would be expected from a hybridization model. This conclusion is thus consistent with previous results on ruby showing that the shift on 10Dq due to $V_R(r)$ can basically be understood through first-order perturbations⁴¹ in which electronic density changes are not involved.

To see how this modulation is induced by the crystal structure of $\text{CaCuSi}_4\text{O}_{10}$, which is the basis of the Egyptian Blue pigment, we have calculated the contribution of the various type of ions present in the lattice to the final potential energy using the Ewald method.³⁹ Using this method, we can calculate the contribution of a particular ion by neutralizing its charge and adding a homogeneous background that compensates for the introduction of charge in the system. This procedure is described in ref 39. The results of this analysis carried out for $\text{CaCuSi}_4\text{O}_{10}$ are depicted in Figure 4. As a salient feature, we can see that the contribution of SiO_4^{4-} units to the total potential energy is dominant over those of Ca^{2+} and Cu^{2+} ions, particularly along the axial direction. Thus, the presence of

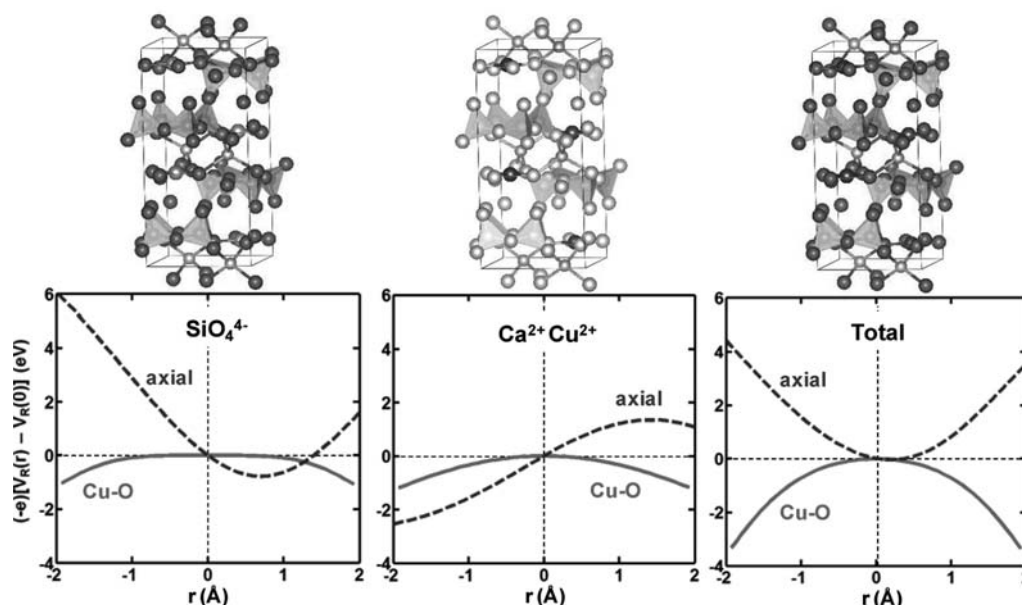


Figure 4. Decomposition of the $(-e)[V_R(r) - V_R(0)]$ potential energy felt by an electron of the CuO_4^{6-} complex in Egyptian Blue ($\text{CaCuSi}_4\text{O}_{10}$). Results are shown when the electron coordinate r moves along either the in-plane Cu–O bond (solid red lines) or the axial OZ (dashed blue lines) direction. The total potential (right) is the sum of the contributions coming from the SiO_4^{4-} units (left) and the Ca^{2+} and Cu^{2+} ions (middle). The positions of the ions that contribute to each potential are highlighted in the structures above each plot. The axial region with $r > 0$ corresponds to the zone placed above the complex in the unit cell of Figure 1 with the lowest value of the Z coordinate. Note that although the contributions from the SiO_4^{4-} units and the Ca^{2+} and Cu^{2+} ions are asymmetric around the Cu^{2+} position, these asymmetries almost compensate for one another when considering the total potential.

SiO_4^{4-} anions in $\text{CaCuSi}_4\text{O}_{10}$ plays a key role in raising the $a_{1g}(3z^2-r^2)$ orbital of CuO_4^{6-} from its position in the zero-field limit. On the other hand, Ca^{2+} and Cu^{2+} ions mainly contribute to the in-plane aspect of the potential that stabilizes the $b_{1g}(x^2-y^2)$ orbital, with an intensity similar to that of the SiO_4^{4-} units. Thus, these results prove that, although SiO_4^{4-} units are not involved in the chromophore itself, manipulation of the crystal structure by the introduction of sand to create $\text{CaCuSi}_4\text{O}_{10}$ is a key step in altering the $(-e)[V_R(\mathbf{r}) - V_R(0)]$ potential and allowing the material to display its characteristic blue hue.

It is worth noting here that although all lattice ions in principle contribute to the embedding potential $(-e)[V_R(\mathbf{r}) - V_R(0)]$, this quantity at variance with $V_R(0)$ actually depends on only a few shells lying nearest to the complex. This idea has been verified in a variety of systems, including $\text{Al}_{2-x}\text{Cr}_x\text{O}_3$,⁴⁵ emerald,⁴¹ $\text{LiBaF}_3:\text{Mn}^{2+}$,⁴⁶ and $\text{MgO}:\text{Cr}^{3+}$.⁴⁷

We will now briefly discuss the origin of the slightly different tonalities shown in Figure 1 by Egyptian Blue ($\text{CaCuSi}_4\text{O}_{10}$) and Han Blue ($\text{BaCuSi}_4\text{O}_{10}$) pigments. Both compounds have isomorphous structures, and the internal potential in both lattices is therefore essentially coincident (Figure S3 in the Supporting Information). Thus, the internal potential $(-e)[V_R(\mathbf{r}) - V_R(0)]$ shifts the levels to open a gap in the blue region for both systems and is key to explaining their color. The slight difference in tonality can be explained by the 0.36% reduction in the Cu–O distance when going from $\text{BaCuSi}_4\text{O}_{10}$ ($R = 1.921 \text{ \AA}$)¹³ to $\text{CaCuSi}_4\text{O}_{10}$ ($R = 1.929 \text{ \AA}$).¹³ Indeed, our DFT calculations predict an increase of 359 cm^{-1} in $E(z^2)$ when changing the Cu–O distance from 1.929 to 1.921 Å, which is in reasonable agreement with the experimental variation of 280 cm^{-1} (Table 1). This situation is thus similar to that found for divalent M^{2+} impurities ($\text{M} = \text{Mn}, \text{Ni}, \text{Co}$) placed in a series of cubic perovskite lattices, such as KMgF_3 or CsCaF_3 . In these cases, variation of the cubic field-splitting parameter 10Dq along the series of isomorphous compounds has been shown to directly reflect the change of the $\text{M}^{2+}-\text{F}^-$ distance.^{40,46} Contrastingly, this idea is no longer true when comparing $\text{KMgF}_3:\text{Mn}^{2+}$ with $\text{LiBaF}_3:\text{Mn}^{2+}$. Although the $\text{Mn}^{2+}-\text{F}^-$ distance is the same for both systems, the 10Dq value is different because the cubic LiBaF_3 has an inverted perovskite structure leading to a $(-e)[V_R(\mathbf{r}) - V_R(0)]$ potential that is quite different from the flat one that corresponds to a normal perovskite structure.⁴⁶

With respect to the Han Purple pigment ($\text{BaCuSi}_2\text{O}_6$) and using ligand field theory,²⁹ we would expect $E(z^2)$ to be smaller than in Egyptian Blue because the Cu–O distance is shorter in the lattice of the latter (Table 1). However, the opposite is true (Table 1), and the internal potential is again indispensable for understanding the color of this system. Because Han Purple is not isomorphous to Egyptian Blue ($\text{CaCuSi}_4\text{O}_{10}$), the internal potential is significantly different for each lattice (Figure 2). For the purple pigment, the small reduction in $E(z^2)$ with respect to the zero-field reference is greatly attributable to the existence of a nearby Cu^{2+} ion along the $+z$ direction (Figure 1) that is not present in $\text{CaCuSi}_4\text{O}_{10}$ (Figure 1), which explains, albeit qualitatively, why this system has a purple tinge.⁴⁸

CONCLUSIONS

The results presented here shed light on the microscopic origin of the bright blue color displayed by the first synthetically produced pigment in human history.^{2–4,9} Moreover, our calculations quantify the large influence of the crystal structure over the optical absorption spectrum of a hosted transition-ion

complex on the basis of the anisotropic internal electrostatic potential $V_R(\mathbf{r})$ created by the lattice. By virtue of this fact, if the same complex was placed in two non-isomorphous insulating lattices, differences in the optical spectra could not be understood if the key role played by $(-e)[V_R(\mathbf{r}) - V_R(0)]$ was ignored, as is often the case in many works involving transition metal cations.^{5–11}

As a salient feature, the results presented here prove that the bright blue color displayed by $\text{CaCuSi}_4\text{O}_{10}$ surprisingly obeys a strong red shift of $\sim 7100 \text{ cm}^{-1}$ of the highest energy d-d transition of the nonembedded CuO_4^{6-} chromophore when exposed to a highly anisotropic internal electrostatic potential. This shift is much higher than those found for 6-fold coordinated complexes located in insulating lattices. For instance, $(-e)[V_R(\mathbf{r}) - V_R(0)]$ gives rise to a blue shift of only 2600 cm^{-1} for the $E(z^2)$ value³¹ corresponding to the CuF_6^{4-} unit in $\text{K}_2\text{ZnF}_4:\text{Cu}^{2+}$. Similarly, the action of this internal potential increases the 10Dq value of ruby by only $\sim 1900 \text{ cm}^{-1}$, which contributes to the red color displayed by this gemstone.⁴¹

The ideas presented here are also useful for obtaining a qualitative understanding of other optical experimental data. For instance, the partial substitution of Ca^{2+} ions in $\text{CaCuSi}_4\text{O}_{10}$ by ions with the same nominal charge (Sr^{2+} , Ba^{2+}) does not lead to significant color changes,⁴⁹ whereas the opposite happens⁵⁰ in $\text{SrCuSi}_4\text{O}_{10}$ through replacing Sr^{2+} by La^{3+} and Cu^{2+} by Li^+ because of a stronger modification to the shape of the electrostatic potential $V_R(\mathbf{r})$. Thus, the ideas presented here allow one to predict what kinds of solid solutions may lead to important color variations with relatively simple electrostatic calculations.

The results of this work in the domain of inorganic chemistry are related to those recently derived for biological chromophores surrounded by proteins.^{51,52} In fact, it has recently been proven⁵¹ that the origins of the different photoabsorptions for the red, green, and blue cone pigments controlling human vision are due to the same retinal chromophore acting under three different electrostatic fields from amino acids of opsin proteins. In the same vein, recent work⁵² has also shown that among the many microenvironmental factors contributing to the color shift of light emission from the firefly luminescent protein applied in bioimaging and biosensors, the primary factor is the electrostatic field produced by several side chains on the chromophore oxyluciferin.

It can be expected that the magnetic and structural properties of insulating transition metal compounds, like optical transitions, also depend on the shape of the internal electrostatic potential $V_R(\mathbf{r})$. Accordingly, it has recently been shown that the different ground state and orbital ordering displayed by La_2CuO_4 and K_2CuF_4 directly reflect distinct electrostatic potentials felt by CuO_6^{10-} and CuF_6^{4-} complexes, respectively, in such lattices.⁵³

Further investigations of the influence of the internal potential $V_R(\mathbf{r})$ on the structural properties of insulating compounds containing transition metal cations are currently under way.

ASSOCIATED CONTENT

Supporting Information

Structure of the Li_2CuO_2 space group, calculated lattice parameters, and influence of $V_R(\mathbf{r})$ on CuO_4^{6-} -containing complexes. This material is available free of charge via the Internet at <http://pubs.acs.org>.

■ AUTHOR INFORMATION

Corresponding Author

*E-mail: garciapa@unican.es.

Notes

The authors declare no competing financial interest.

■ ACKNOWLEDGMENTS

This work was supported by the Spanish Ministerio de Economía y competitividad under Projects FIS2012-30996 and FIS2012-37549-C05-4. P.G.-F. acknowledges funding from the Ramon y Cajal program.

■ REFERENCES

- (1) Buxbaum, G., Ed. *Industrial Inorganic Pigments*; Wiley-VCH: Weinheim, Germany, 1998.
- (2) Pastoureaux, M. *Blue: The History of a Color*; Princeton University Press: Princeton, NJ, 2001.
- (3) Berke, H. *Angew. Chem., Int. Ed.* **2002**, *41*, 2483–2487.
- (4) Berke, H. *Chem. Soc. Rev.* **2007**, *36*, 15–30.
- (5) Nassau, K. *The Physics and Chemistry of Color*; Wiley: New York, 1983.
- (6) Burns, R. G. *Mineralogical Applications of Crystal-Field Theory*; Cambridge University Press: Cambridge, U.K., 1993.
- (7) Tilley, R. *Colour and the Optical Properties of Materials*; Wiley: West Sussex, U.K., 2011.
- (8) Clark, M. G.; Burns, R. G. *J. Chem. Soc. A* **1967**, 1034–1038.
- (9) Ford, R. J.; Hitchman, M. A. *Inorg. Chim. Acta* **1979**, *33*, L167–L170.
- (10) Reinen, D.; Atanasov, M.; Nikolov, G.; Steffens, F. *Inorg. Chem.* **1988**, *27*, 1678–1686.
- (11) Moretti Sala, M.; Bisogni, V.; Aruta, C.; Balestrino, G.; Berger, H.; Brookes, N. B.; de Luca, G. M.; Di Castro, D.; Griioni, M.; Guarise, M.; Medaglia, P. G.; Miletto Granozio, F.; Minola, M.; Perna, P.; Radovic, M.; Salluzzo, M.; Schmitt, T.; Zhou, K. J.; Braicovich, L.; Ghiringhelli, G. *New J. Phys.* **2011**, *13*, 043026.
- (12) Warner, T. E. *Synthesis, Properties and Mineralogy of Important Inorganic Materials*; Wiley: West Sussex, U.K., 2011.
- (13) Chakoumakos, B. C.; Fernandez-Baca, J. A.; Boatner, L. A. *J. Solid State Chem.* **1993**, *103*, 105–113.
- (14) At the fall of the Roman Empire, knowledge of the Egyptian Blue technology disappeared almost abruptly, the last written reference being in the *Etymologiae* from Saint Isidore of Seville (s. VII). However, recent works have found that this pigment appears in some Byzantine frescos (s. IX), a Roman church in Spain (s. XI), and some Cinquecento paints in Bologna (s. XVI): McCouat, P. *Egyptian Blue: The Colour of Technology. Journal of Art in Society*. www.artinsociety.com (accessed 2014).
- (15) The similarities among Egyptian Blue, Han Blue, and Han Purple pigments led some to suggest that Han Blue was based on Egyptian Blue knowledge, which had travelled east along the Silk Road.² Other works maintain that both technologies were developed independently: Liu, Z.; Mehta, A.; Tamura, N.; Pickard, D.; Rong, B.; Zhou, T.; Pianetta, P. *J. Archaeol. Sci.* **2007**, *34*, 1878. This subject is currently a hot topic in art and archeology research of ancient pigments.
- (16) Sparta, K. M.; Roth, G. *Acta Crystallogr., Sect. B: Struct. Sci.* **2004**, *60*, 491–495.
- (17) When exposed to visible light, CaCuSi₄O₁₀ emits a strong near-infrared light with high efficiency and a long lifetime, making it appealing for several applications in the fields of biomedical analysis, telecommunications, and lasers.^{18,19} Moreover, the exfoliation of CaCuSi₄O₁₀ into nanosheets and nanoplatelets under simple reaction conditions has provided a route to a new class of two-dimensional nanomaterials with applications in medical imaging, security ink, optical fibers, and light-emitting diodes.²⁰ The Han Purple pigment is also the object of great interest from the observation of a Bose–Einstein condensation of spin-excitations at temperatures up to ~5 K using magnetic fields $H > 30$ T.²¹
- (18) Accorsi, G.; Verri, G.; Bolognesi, M.; Armaroli, N.; Clementi, C.; Miliani, C.; Romani, A. *Chem. Commun. (Cambridge, U.K.)* **2009**, 3392–3394.
- (19) Borisov, S. M.; Würth, C.; Resch-Genger, U.; Klimant, I. *Anal. Chem.* **2013**, *85*, 9371–9377.
- (20) Johnson-McDaniel, D.; Barrett, C. A.; Sharafi, A.; Salguero, T. *J. Am. Chem. Soc.* **2013**, *135*, 1677–1679.
- (21) Sebastian, S. E.; Harrison, N.; Batista, C. D.; Balicas, L.; Jaime, M.; Sharma, P. A.; Kawashima, N.; Fisher, I. R. *Nature* **2006**, *441*, 617–620.
- (22) Karpinski, J.; Schwer, H.; Mangelschots, I.; Conder, K.; Morawski, A.; Lada, T.; Paszewin, A. *Physica C* **1994**, *234*, 10–18.
- (23) Chung, E. M. L.; McIntyre, G. J.; McK. Paul, D.; Balakrishnan, G.; Lees, M. R. *Phys. Rev. B* **2003**, *68*, 144410.
- (24) Botto, I. L.; Baran, E. J.; Minelli, G. *An. Asoc. Quim. Argent. (1921-2001)* **1987**, *75*, 429.
- (25) Chen, Y.; Zhang, Y.; Feng, S. *Dyes Pigm.* **2014**, *105*, 167–173.
- (26) Rosner, H.; Johannes, M. D.; Drechsler, S.-L.; Schmitt, M.; Janson, O.; Schnelle, W.; Liu, W.; Huang, Y.-X.; Kniep, R. *Sci. Technol. Adv. Mater.* **2007**, *8*, 352–356.
- (27) Maekawa, S.; Tohyama, T.; Barnes, S. E.; Ishihara, S.; Koshibae, W.; Khaliullin, G. *Physics of Transition Metal Oxides*; Springer-Verlag: Heidelberg, Germany, 2004.
- (28) Schön, J. H.; Dorget, M.; Beuran, F. C.; Zu, X. Z.; Arushanov, E.; Deville Cavellin, C.; Laguës, M. *Nature* **2001**, *414*, 434–437.
- (29) Jørgensen, C. K. *Modern Aspects of Ligand Field Theory*; North-Holland: Amsterdam, 1971.
- (30) McDonald, R. G.; Hitchman, M. A. *Inorg. Chem.* **1986**, *25*, 3273–3281.
- (31) García-Fernandez, P.; Barriuso, M. T.; García-Lastra, J. M.; Moreno, M.; Aramburu, J. A. *J. Phys. Chem. Lett.* **2013**, *4*, 2385–2390.
- (32) CRYSTAL09 Basis Sets. http://www.crystal.unito.it/Basis_Sets/Ptable.html.
- (33) Peintinger, M. F.; Vilela Oliveira, D.; Bredow, T. *J. Comput. Chem.* **2013**, *34*, 451–459.
- (34) Bilc, D. I.; Orlando, R.; Shaltaf, R.; Rignanese, G.-M.; Íñiguez, J.; Ghosez, Ph. *Phys. Rev. B* **2008**, *77*, 16510.
- (35) Bredow, T.; Gerson, A. *Phys. Rev. B* **2000**, *61*, 5194–5201.
- (36) Becke, A. D. *J. Chem. Phys.* **1993**, *98*, 5648–5652.
- (37) te Velde, G.; Bickelhaupt, F. M.; Baerends, E. J.; Fonseca Guerra, C.; van Gisbergen, S. J. A.; Snijders, J. G.; Ziegler, T. *J. Comput. Chem.* **2001**, *22*, 931–967.
- (38) van Gool, W.; Piken, A. G. *J. Mater. Sci.* **1969**, *4*, 95–104.
- (39) Tosi, M. P. *Solid State Phys.* **1964**, *16*, 1–120.
- (40) Moreno, M.; Barriuso, M. T.; Aramburu, J. A.; García-Fernandez, P.; García-Lastra, J. M. *J. Phys.: Condens. Matter* **2006**, *18*, R315–R360.
- (41) Aramburu, J. A.; García-Fernandez, P.; García-Lastra, J. M.; Barriuso, M. T.; Moreno, M. *Phys. Rev. B* **2012**, *85*, 245118.
- (42) Gaudry, E.; Cabaret, D.; Brouder, C.; Letard, I.; Rogalev, A.; Wilhem, F.; Jaouen, N.; Sainctavit, P. *Phys. Rev. B* **2007**, *76*, 094110.
- (43) (a) Gerloch, M.; Harding, J. H.; Wooley, R. G. *Struct. Bonding (Berlin, Ger.)* **1981**, *46*, 1–46. (b) Deeth, R. J.; Gerloch, M. *Inorg. Chem.* **1984**, *23*, 3846–3853. (c) Deeth, R. J.; Foulis, D. L. *Phys. Chem. Chem. Phys.* **2002**, *4*, 4292–4297. (d) Deeth, R. J.; Anastasi, A.; Diedrich, C.; Randell, K. *Coord. Chem. Rev.* **2009**, *253*, 795–816. (e) Deeth, R. J. *Molecular Modelling for Systems Containing Transition Metal Centres*. In *Structure and Function*; Comba, P., Ed.; Springer: Dordrecht, The Netherlands, 2010. (f) Reinen, D.; Atanasov, M.; Lee, S.-L. *Coord. Chem. Rev.* **1998**, *175*, 91–158.
- (44) Our opinion on the use of parametrized models to interpret transition metal spectra is well illustrated in the preface of the book *Molecular Electronic Structures of Transition Metal Complexes* by one of the forefathers of ligand field theory, Carl Ballhausen: “Unfortunately, the temptation is to elaborate an approximate theory and to introduce an increasing number of loosely defined ‘effects’ in order to ‘explain’

the movements of the parameters... there is little reason to expect that deeper insight can be gained in this way.”

(45) García-Lastra, J. M.; Barriuso, M. T.; Aramburu, J. A.; Moreno, M. *Phys. Rev. B* **2009**, *79*, R241106.

(46) Trueba, A.; García-Lastra, J. M.; Barriuso, M. T.; Aramburu, J. A.; Moreno, M. *Phys. Rev. B* **2008**, *78*, 075108.

(47) Aramburu, J. A.; García-Fernandez, P.; García-Lastra, J. M.; Barriuso, M. T.; Moreno, M. *J. Phys.: Condens. Matter* **2013**, *25*, 175501.

(48) Berke⁴ has recently noted that pure Han Purple is “not purple in its pure state, but dark blue. The purple shade of Han Purple comes from the red impurity of copper(I) oxide, Cu₂O.” In this work, we show that the internal potential $V_R(\mathbf{r})$ allows for a gap to open in the higher part of the optical spectrum for Han Purple that is smaller than that for Egyptian Blue. This is consistent with a more purple/deeper blue color for Han Purple. However, accounting for effects such as the proximity of the dimer or the influence of Cu₂O in the color is beyond the scope of the present work.

(49) Kendrick, E.; Kirk, C. J.; Dann, S. E. *Dyes Pigm.* **2006**, *73*, 13–18.

(50) Jose, S.; Reddy, M. L. *Dyes Pigm.* **2013**, *98*, 540–546.

(51) Fujimoto, K.; Hasegawa, J.; Nakatsuji, H. *Chem. Phys. Lett.* **2008**, *462*, 318–320.

(52) Cai, D.; Marques, M. A. L.; Nogueira, F. *J. Phys. Chem. B* **2013**, *117*, 13725–13730.

(53) García-Fernandez, P.; Moreno, M.; Aramburu, J. A. *J. Phys. Chem. C* **2014**, *118*, 7554–7561.